**Title**: Kit Ligand and Kit receptor tyrosine kinase sustain synaptic inhibition of Purkinje Cells.

**Authors/Affiliation**

Tariq Zaman[1]

Daniel Vogt[1]

Jeremy Prokop[2]

Qusai Abdulkhaliq Alsabia[1]

Gabriel Simms[1]

April Stafford[1]

Bryan W. Luikart[3]

Michael R. Williams*[1]

1: Department of Pediatrics & Human Development, College of Human Medicine, Michigan State University

2: Office of Research, Corewell Health

3: Department of Molecular and Systems Biology, Geisel School of Medicine at Dartmouth College

**Correspondence:** will3434@msu.edu

**Keywords** Kit Ligand, Kit Receptor Tyrosine Kinase, Cerebellum, GABAergic Synapse

**Funding NIH/NIMH** K99/R00 MH110665

**Summary:** The cell-type specific expression of ligand/receptor and cell-adhesion molecules is a fundamental mechanism through which neurons regulate connectivity. Here we determine a functional relevance of the long-established mutually exclusive expression of the receptor tyrosine kinase Kit and the trans-membrane protein Kit Ligand by discrete populations of neurons in the mammalian brain. Kit is enriched in molecular layer interneurons (MLIs) of the cerebellar cortex (i.e., stellate and basket cells), while cerebellar Kit Ligand is selectively expressed by a target of their inhibition, Purkinje cells (PCs). By *in vivo* genetic manipulation spanning embryonic development through adulthood, we demonstrate that PC Kit Ligand and MLI Kit are required for, and capable of driving changes in, inhibition of PCs. Collectively, these works in mice demonstrate that the Kit Ligand/Kit receptor dyad sustains mammalian central synapse function and suggest a rationale for the affiliation of Kit mutation with neurodevelopmental disorders.

**Visual Abstract**

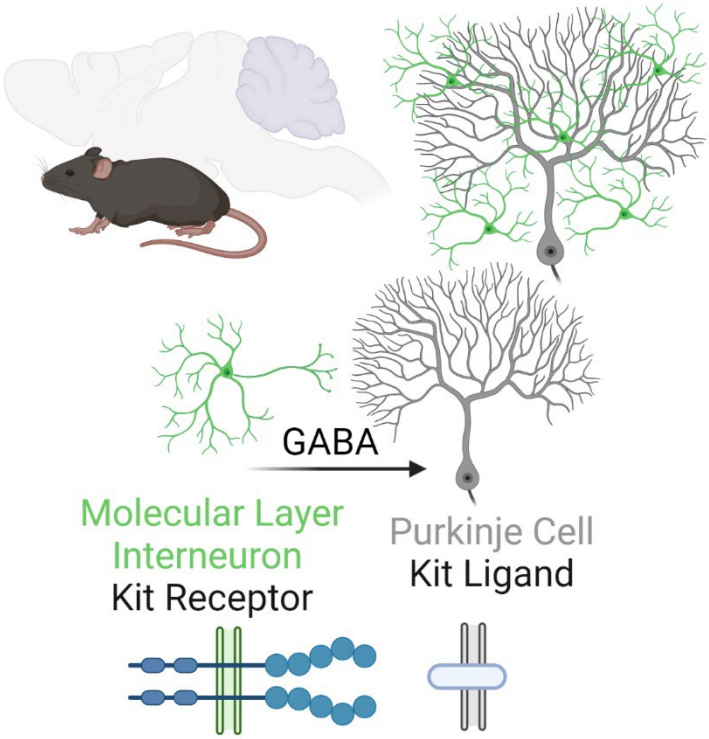

## Introduction

The proto-oncogene receptor tyrosine kinase Kit (c-Kit, CD117) is an evolutionarily conserved, loss-of-function intolerant, gene that is enriched in specific neuron populations and tentatively associated with rare cases of neurological dysfunction (pLI= 0.98 and LOEUF of 0.17) (**Figure S1A,B**)[1,2]. It is perhaps unsurprising that loss-of-function Kit mutations in humans are rare; Kit is highly pleiotropic, supporting diverse cell populations including melanocytes, hematopoietic stem/progenitor cells, germ cells, masts cell, and interstitial cells of Cajal[3]. Thus, Kit mutations can result in diverse conditions such as hypo- or hyperpigmentation or melanoma, anemia or leukemia, infertility, mastocytosis, and impaired gut motility or gastro-intestinal tumors (Kit biology reviewed [2 4]).

The activation of Kit is stimulated by Kit Ligand (Gene symbol is KITLG, herein KL), a single-pass transmembrane protein having an extracellular active domain that induces Kit dimerization and kinase activity. Across several decades and species, it has been reported that KL and Kit are mutually expressed in discrete neuron populations known to be connected; it has thus been hypothesized that the expression pattern of KL-Kit may reflect a role in connectivity[5-8]. Consistent with such a function, case reports have implicated inactivating Kit mutations with neurological impairment (References[9-13] and **Figure S1C**). Clinical phenotypes include developmental delay, ataxia, hypotonia, intellectual disability, deafness, and autism spectrum disorder. White matter abnormalities have been noted, and limited evidence suggests KL-Kit may indeed regulate axon outgrowth. KL or Kit mutation or pharmacological manipulation alters outgrowth of spinal commissural axons *in vitro*[14], KL stimulates cortical neurite outgrowth *in vitro* [15], and Kit reduction in cortex of developing rats or mice delays axon extension[16]. While these reports provide anatomical/morphological data suggesting that KL-Kit influences connectivity, critically, these studies did not address functional consequences to neuronal physiology or synaptic connectivity. Functional studies of KL-Kit in synaptic physiology have likely been hampered by pleiotropy and organismal or cell death. Severe global KL-Kit hypomorphs exhibit fatal anemia, and developmental Kit depletion or inhibition in the cerebrum has resulted in death of neuronal progenitors or nascent neurons[16-18]. Therefore, whether KL-Kit is necessary for synaptic function has remained largely unstudied. Here, we address this gap.

In mice, rats, and humans, Kit is abundantly expressed by molecular layer interneurons (MLIs) of the cerebellar cortex[6-8,19], while cerebellar KL is restricted to Purkinje Cells (PCs), which MLIs provide GABAergic synaptic inhibition to. We tested the hypothesis that PC KL and MLI Kit were essential to the GABAergic inhibition of PCs. We created a Kit conditional knockout mouse and accomplished embryonic knockout of Kit from all MLIs; separately, we knocked out KL from postnatal PCs. By either method, disruption of the KL-Kit ligand-receptor pair produced robust and specific impairments to GABAergic inhibition of PCs. Through sparse postnatal viral manipulation of KL in PCs, we provide evidence that KL functions throughout adulthood to regulate synaptic function. These results demonstrate that cell-type specific expression of KL and Kit influences functional connectivity in the mammalian brain, informing the long-observed expression of KL-Kit in the brain and suggesting a rationale for the affiliation of Kit loss with neurological impairment.

## Methods

Animals: All procedures performed at Michigan State University were approved by the Institutional Animal Care and Use Committees of Michigan State University, which is accredited by the Association for Assessment and Accreditation of Laboratory Animal Care (AAALAC). Mice were on a 12-hour dark/light cycle, with ad libitum food and water. Male and female mice were used for all experiments. Mice were genotyped in-house using standard PCR-based methods, or via Transnetyx.

Creation of Kit conditional knockout mouse: We generated a strain of mice having exon 4 of Kit floxed. This was accomplished by utilizing the services of UNC Animal Models Core (Dr. Dale Cowley) to generate chimeras from an ES cell line having a Knockout-first Allele (with conditional potential) for Kit (HEPD0509_8). The ES clones were obtained through the EuMMCR (European Mouse Mutant Cell Repository) of the EUCOMM (European Conditional Mouse Mutagenesis Program)[20]. Chimeric mice were screened for germline transmission of the targeted allele and were then crossed to a Flp deleter strain (C57BL/6N-Albino-Rosa26-Flpo) to convert the knockout-first allele to a conditional allele (tm1c) through removal of the FRT-flanked selection cassette. F1 male offspring carrying Kit tm1c and Flp alleles were crossed to C57Bl6/J females; we selected resultant progeny heterozygous for Kit tm1c but negative for Flp and the selection cassette. The Kit tm1c alle was bred to homozygosity while selecting against animals carrying the Tyr c-Brd allele (previously conveyed by C57BL/6N-Albino-Rosa26-Flpo). The strain of mice having the Kit floxed tm1c allele are given the nomenclature

C57BL/6N−Kit$^{tm1c(EUCOMM)Mirow}$/J; the Mirow lab code is provisional. Additional strains of mice used were Pax2-Cre transgenic mice (STOCK Tg(Pax2-cre)1Akg/Mmnc, RRID:MMRRC_010569-UNC[21], Kit eGFP (Tg(Kit-EGFP)IF44Gsat/Mmucd; Gensat) [22] backcrossed for greater than 5 generations to C57Bl6/J (Stock No: 000664, The Jackson Laboratory), KitL floxed (Kitltm2.1Sjm/J, Stock #017861) [23], and Pcp2-Cre (Stock # 004146) mice [24], all from The Jackson Laboratory.

To produce mixed litters of "Control" and "Kit KO" animals, mice homozygous for the Kit tm1c allele but negative for Pax2-Cre were crossed to mice homozygous for the floxed allele and Pax2-Cre positive. We used Kit KO females crossed to Control males as our breeding scheme. Experimental animals were derived from at least 5 generations of backcrossing Kit KO animals to Kit tm1c homozygous animals derived from a separate (Kit tm1c homozygous x Kit tm1c homozygous) breeding cohort.

Validation of Kit knockout: We investigated conditional knockout of Kit protein from the cerebellum by Western blot of total protein lysates from acutely harvested cerebellums (~P52) and by indirect immunofluorescence on free-floating vibratome-generated sections of transcardial-perfused formaldehyde-fixed mouse brains (~P31). Western blots were probed with Rabbit: α-Kit (clone D13A2, Cell Signaling Technologies product 3074), α-GAPDH (Clone 14C10, product 2118 Cell Signaling Technology), or α-parvalbumin antibody (product PV-27, Swant), each primary was detected via HRP conjugated Goat α-Rabbit secondary antibody (Biorad, product 170-6515) after incubation with Clarity ECL substrate (Bio-Rad, 1705061) via a BioRad ChemiDoc MP.

For indirect immunofluorescence, primary antibodies were rat α-Kit (Rat α-Kit clone ACK4, ThermoFisher, product MA5-17836), mouse α-calbindin (α-calbindin-D28K, CB-955, Sigma Aldrich), and rabbit α-parvalbumin (PV-27, Swant). Primaries were detected by Goat-host highly cross-adsorbed secondary antibodies coupled to Alexa 488, Cy3, or Alexa 647 (Jackson Immunoresearch). Nuclei were labeled with DAPI, tissues were mounted in an anti-fade reagent, and fluorescent signals captured laser scanning confocal microscopy. Cell densities for MLIs (parvalbumin positive and/or calbindin negative somas of the molecular layer) were performed on Maximum Z-projections of 2.5-2.6 micron thick stacks, using the multi-point feature for counting somas, and the polygon ROI tool for determining the area of the Molecular Layer in which the somas were counted; results from two-technical replicates were averaged for each animal. The polygon tool was also used for determining maximal PSD95+ pinceau area. To determine the width of the molecular layer, seven linear ROIs per field of view of comparable locations of lobules IV/V were averaged to generate per animal layer thickness measurements. For analysis of synapses, we quantified puncta in the molecular layer that were triple positive for rabbit α-VGAT(131 003), mouse α-Gephyrin (147 011), and Chicken α-Calbindin (214 006), all from Synaptic Systems. For analysis of pinceau markers we utilized mouse α-Kv1.1 (K36/15), Kv1.2 (K14/16), and PSD-95 (K28/43), all from NeuroMab/AntibodiesInc.

Stereotaxic Procedures: Injections of replication-defective viral particles used protocols substantially similar to those previously published [25]. In brief, mice were brought to an anesthetic plane using inhaled isoflurane by a low-flow system (SomnoSuite, Kent); thermal regulation was assisted by heating pad, and pain managed through topical lidocaine and ketoprofen. A digital stereotaxic device (Kopf) and reference atlas were used to localize a small hole in the skull; cerebellar coordinates were: neonates; A/P, -2.55; M/L, - 1.1 (reference Lambda), D/V, 1.5 to 0.5 from dura; juvenile; A/P, -6.25; M/L, - 1.35; D/V, 1.5 to 0.75 (reference Bregma); adults; A/P, -6.35; M/L, - 1.8; D/V, 1.5 to 0.75 (reference Bregma). Viral particles were delivered via a ~30-gauge Hamilton Syringe controlled by digital syringe pump (WPI). Virus volume was 1-2 ul and there was a 5-minute period after infusion prior to needle withdrawal. Animals were monitored during and after surgical operations. Ages for injection were, nominally, postnatal day (P) 7, 19, and 56; for P7 and P19, variability of up to two days was utilized to accommodate differences in animal size, and for P56 the eighth week of life was utilized.

Viruses: Lentiviral particles were derived from vectors previously described to express transgenes under the hUbiC promoter and pseudotyped with VSV-G [26,27]. Silent mutations disrupted the internal EcoRI sites of mouse KitL (MC204279, Origene), the KitL coding sequence was then flanked by EcoRI sites, and the subsequent KitL coding sequence was introduced into a FUC-T2A-(EcoRI) plasmid, to create a FUC-T2A-KL-1 plasmid, wherein C designates mCherry. Subsequent deletion of KitL Exon 6 generated a KL-2 vector [28-31]. Sequences were verified by sequencing. Adeno-Associated Viral (AAV) particles were created by Vigene to drive Cre expression

by the Purkinje Cell-Specific L7.6 promoter [32], or to drive mCherry or mCherry-T2A-KL-2 in a Cre-On fashion under the EF1α promoter, with the AAV1 serotype.

Electrophysiology: For patch clamp electrophysiology of Control vs Kit KO, cells were recorded in slices generated from animals at 36.9 ± 0.6 and 37.4 ± 0.9 days for MLIs and PCs respectively. Avertin-anesthetized mice were perfused with a carbogen-equilibrated ice-cold slicing solution containing (in mM): 110 $C_5H_{14}ClNO$, 7 $MgCl_2.6H_2O$, 2.5 KCl, 1.25 $NaH_2PO_4$, 25 $NaHCO_3$, 0.5 $CaCl_2$-$2H_2O$, 10 Glucose, and 1.3 Na-Ascorbate. In the same solution, we generated 250-micron thick parasagittal sections of the cerebellum (Leica VT1200). Slices recovered at 34°C for 30 minutes in a carbogenated ACSF containing (in mM): 125 NaCl, 25 $NaHCO_3$, 1.25 $NaH_2PO_4$, 2.5 KCl, 1 $MgCl_2.6H_2O$, 1 $CaCl_2$-$2H_2O$ and 25 Glucose; slices were then held at room temperature for at least 30 minutes before recording. Recordings were performed in carbogenated external recording ACSF (32.7 ± 0.1°C) containing (in mM): 125 NaCl, 25 $NaHCO_3$, 1.25 $NaH_2PO_4$, 2.5 KCl, 1 $MgCl_2.6H_2O$, 2 $CaCl_2$-$2H_2O$ and 25 Glucose. MLIs and PCs of folia IV/V were targeted for recording by IR-DIC, or epifluorescence stimulated by a CoolLED pE-4000, detected via a SciCam Pro on a SliceScope Pro 6000-based rig (Scientifica). Recording electrodes were pulled (Narishige, PC-100) from standard-wall borosilicate glass capillary tubing (G150F-4, Warner Instruments) and had 5.1 ± 0.08 and 2.8 ± 0.02 MΩ tip resistance for MLIs and PCs respectively. Spontaneous Inhibitory Postsynaptic Currents (sIPSCs) and Miniature Inhibitory Postsynaptic Currents (mIPSC) were recorded with an intracellular solution containing (in mM):140 CsCl, 4 NaCl, 0.5 $CaCl_2$-$2H_2O$, 10 HEPES, 5 EGTA, 2 Mg-ATP, and 0.4 Na-GTP, 2 QX-314. For action potential recordings and for Miniature Excitatory Postsynaptic Currents (mEPSCs), the intracellular solution contained (in mM): 140 K-gluconate, 10 KCl, 1 $MgCl_2$, 10 HEPES, 0.02 EGTA, 3 Mg-ATP, and 0.5 Na-GTP as described previously [33]. The internal pipette solution pH was adjusted to 7.35 with CsOH for IPSCs and mIPSCS, and with KOH for mEPSCs and action potentials, while for all the osmolarity was adjusted to 300 mOsmolL-1 with sucrose. In whole-cell voltage clamp mode PCs were held at -70 mV; to isolate sIPSCs, NBQX (10 μM) and D-AP5 (50 μM) were added to the recording solution and mIPSCs recordings additionally included 1 μM tetrodotoxin (TTX). To record mEPSCs, 1 μM TTX and 50 μM picrotoxin was added to extracellular solution. Action potentials were recorded in MLIs within the middle third of the molecular layer; spontaneous action potentials were recorded in I=0 mode, or action potentials were evoked by depolarizing current injection in 600 ms steps of 10 pA, from 0 to 150 pA, with a 7 second inter-sweep interval. For paired pulse, current ranging from 150 uA to 250uA was delivered by concentric bipolar stimulating electrode in the molecular layer. Stimulus duration was 50 microseconds, and ISI was 50 mS. For each cell, 10 sweeps were recorded with 10 S inter sweep interval. Purkinje Cells with an access resistance of 10-20 (15.9 ± 0.5), or MLIs with an access resistance <30 (23.6 ± 0.6) MΩ were considered for recording. Recordings with >20% change in series resistance were excluded from analysis. Signals were acquired at 10 KHz with a low-noise data acquisition system (Digidata 1550B) and a Multiclamp700-A amplifier and were analyzed using pClamp11.1 (Molecular Devices). Both mIPSCs and mEPSCs with over 8 pA amplitude and longer than 1 ms duration were included while overlapping events were rejected from analysis; also rejected from analysis was any miniature event for which amplitude, rise, and decay metrics were not all available. Analysis of the PCP2 Cre mediated KL KO tissues was conducted similarly at ~40-44 days old. For viral PC KL KO animals injected as neonates (P7), juvenile (P19), and adults (P56) were recorded at an average of ~35, 45, and 83 days old, respectively.

Software: Microscopic image processing was conducted via FIJI/ImageJ, electrophysiological data was analyzed by pClamp11.1, statistical analyses were conducted via GraphPad Prism 9, and Fig.s were created with BioRender, PowerPoint, and GraphPad Prism 9.

## Results

We generated mice in which Kit exon 4 is flanked by LoxP sites (Kit tm1c); Kit gene modifications are illustrated in **Figure 1A, B.** Kit tm1c homozygous Control animals had normal appearance, sex ratios, and reproductive success. Kit is abundantly expressed in GABAergic interneurons in the molecular layer of the cerebellar cortex (MLIs), whereas Kit Ligand (KL) is expressed by Purkinje cells (PCs). To determine if Kit influences synapse function, we conditionally knocked out Kit from MLIs and assessed the MLI-PC synapse. Pax2 is a transcription factor expressed early in the lineage of GABAergic interneurons of the cerebellum[34]; a Pax2-Cre transgene enables embryonic recombination[35,36]. We generated Kit tm1c homozygous litters of which nominally half were hemizygous for Pax2 Cre (Kit KO) and half were not (Control) **Figure 1C.** We produced Control and Kit KO animals in normal sex and genotype ratios. As expected for the C57Bl6/J background, Control littermates had

dark coat and eyes, but littermate Kit KO animals had white whiskers, white fur with variable pigmented patches, and black eyes; example littermates **Figure 1D.** Given Pax2 expression in melanocytes[37] and the role of Kit in melanogenesis (Reviewed in[38,39]), the pigmentation phenotype provided gross confirmation of conditional Kit KO. We thus confirmed that cerebella of Kit KO animals were Kit depleted. By immunohistochemistry in Control animals, we recapitulated the known pattern of Kit immunoreactivity in the parvalbumin positive MLIs of the cerebellar cortex (**1F and Inset**). In contrast, a sex-matched Kit KO littermate demonstrated loss of cerebellar Kit immunoreactivity. By Western blot of cerebellar lysates from Control animals, Kit resolved as a major band at ~120 kD, but in Kit KO littermates, Kit immunoreactivity was lost; GAPDH as loading control was equivalent, as was parvalbumin (which marks mature MLIs and PCs) **Figure 1G**.

Having validated that Kit KO animals lacked cerebellar Kit, we assessed the functional impact. We compared spontaneous GABAergic inhibitory post synaptic currents (sIPSC) in PCs of acute slices generated from ~P34 Control and Kit KO animals, schema **Figure 2A**, example traces **Figure 2B**. Kit KO was associated with a significant change in the distribution of sIPSC event amplitudes (**Figure 2C**). Calculating average sIPSC event frequency, amplitude, and duration for each PC of Control or Kit KO revealed a significant decrease in sIPSC frequency (**1D**) but not amplitude or duration. The reduced sIPSC frequency in Kit KO was not associated with changes in density or distribution of MLIs or in thickness of the molecular layer (**Figure S2)**.

We sought to determine if reduced PC inhibition was related to altered MLI physiology (Schema, **Figure S3A**). Capacitance, input resistance, and spontaneous or stimulated MLI action potential frequency was not different between Control and Kit KO (**Figure S3B-E)**. Since MLIs were present and firing normally in Kit KO, we sought to determine if there were defects in evoked neurotransmitter release. Direct electrode stimulation of the outer or inner molecular layer in a paired-pulse paradigm (Schema, **Figure S3F**) evoked IPSCs of equivalent amplitude in PCs from Control and Kit KO, and we detected no difference in the paired pulse ratio (**Figure S3G,H**). These data suggest that MLI synapses could function normally in Kit KO under direct stimulation. We therefore investigated markers of the MLI:PC synapses to determine if they were altered.

The density of GABAergic synapses upon PCs (triple positive VGAT, Gephyrin, and Calbindin puncta in the molecular layer) was not reduced by Kit KO (example immunofluorescence, **Figure S4A**). However, GABAergic puncta upon PCs were significantly smaller (~10%) in Kit KO (**Figure S4B**). MLI axon terminals contribute not just to individual axo-dendritic synaptic puncta, but also to interdigitated MLI axon collaterals around the soma and initial axon segment of PCs, forming “pinceaux” structures. By parvalbumin immunoreactivity, these structures were preserved but smaller in Kit KO (arrowheads **Figure S4C)**, and this was confirmed by decreased Kv1.2 (**Figure S4D**) and PSD95 (**Figure S4D**). As PSD95 immunoreactivity faithfully follows multiple markers of pinceaux size [40], we quantified PSD95 immunoreactive pinceau area and determined that pinceaux area was decreased by ~50% in Kit KO (n 26 Control vs 43 Kit KO, $p<0.0001$, two-tailed t-test). These results suggested that Kit KO MLIs may have defects in physical and/or functional maturation of synapses upon PCs.

To evaluate the number of functional GABAergic synapses, we analyzed miniature synaptic currents in acute cerebellar slices, (schema **Figure 2 E,F,G**; example traces **Figure 2 H,I,J)**. In PCs of Kit KO, there was a significant ~50% reduction in the average frequency, but not amplitude, of mIPSCs (**Figure 2K**). In contrast, the average frequency and amplitude of mEPSCs in PCs from Control and Kit KO did not differ (**Figure 2L**). These data suggested that Kit KO impaired the MLI:PC synapse but did not rule out a general defect in MLI synapse function. As MLIs synapse not just upon PCs, but also upon MLIs, we evaluated mIPSCs in MLIs. Mean mIPSC frequency and amplitude was unchanged between Control and Kit KO (**Figure 2M**). Therefore, embryonic MLI Kit KO was associated with a specific defect in the number or proportion of functional GABAergic synapses upon PCs. As MLI Kit and PC KL expression is maintained postnatally, we hypothesized that postnatal postsynaptic PC KL KO would phenocopy embryonic presynaptic MLI Kit KO.

We utilized previously described KL floxed[23] and PC-Cre[24] strains to yield mice with Control or KL KO PCs (Schema **Figure 3A**). We confirmed depletion of cerebellar KL transcripts by rtPCR in data not shown[23], and we confirmed that PC KL KO did not disrupt the pattern of Kit immunoreactivity. Patch clamp of PCs in acute slices revealed that PC KL KO produced significant differences in the distribution of sIPSC event amplitudes (Example traces **Figure 3B, Figure 3C**). PC KL KO reduced the average sIPSC frequency, amplitude, and duration in PCs (**Figure 3D**). The phenotype was specific to GABAergic synapses: there was a substantial reduction in the frequency but not the amplitude of mIPSC events in PCs (**Figure 3E**). In contrast, frequency and amplitude of mEPSCs in KL KO PCs was not different (**Figure 3F**). In data not shown, a KS test revealed a significant difference in the individual mEPSC event amplitude distribution ($p=0.0002$, n=1196 Control vs 1244 KL KO), however the mean mEPSC amplitude was within 1% between conditions. Similarly, a KS test of mIPSC event

amplitudes revealed a significant difference ($p<0.0001$, n=5996 Control vs 3958 KL KO), but the mean mIPSC amplitude was ~10% greater in PC KL KO than in Control. It is therefore unlikely that decreased event amplitude contributed to the specific and robust >50% decrease in mIPSC frequency detected in PC KL KO. Thus, like MLI Kit KO, PC KL KO reduced inhibition of PCs.

Recombination by PCP2 Cre begins at ~P7[24] , whereas Pax2 Cre recombination occurs at ~E15 [21,34]. Our results thus suggest that continued expression of the KL-Kit dyad sustains inhibitory drive to PCs. To test this hypothesis (and avoid transformative effects of Kit overexpression), we tuned KL postnatal expression *in vivo.*

To determine if acute focal manipulations in KL modulate PC inhibition, we injected replication-defective viruses leveraging the PC-specific L7.6 promoter[32] to express Cre in KL floxed animals, and we identified Cre-positive PCs by mCherry expression (Schema **Figure 4A**, Example transduction, **Figure S5A-C,F-H**). Injections were at P7, P18, or P56; acute slices were generated 2-3 weeks later. Patch-clamp recordings in areas of sparse infection revealed that regardless of when KL was depleted, PC KL KO reduced PC sIPSC frequency (P7, P18, and P56 in **Figure S5,** P18 injections **Figure 4C,D)**. We next examined PC KL over-expression. We co-injected L7.6 Cre AAV with AAV encoding EF1α driven Cre-on mCherry and the membrane bound isoform of mouse KL (mKL2) via a T2A element to produce PC KL overexpression (OX) (Schema **Figure 4B**). Whether at P18 or P56, KL OX PCs had increased sIPSC frequency and amplitude compared to nearby Control PCs (**Figure 4E,F**).

We noted that Control PCs from the PC KL KO paradigm had sIPSC frequency and amplitude similar to PCs from Sham injections (**Figure 4C,4D**). In contrast, while KL OX PCs received elevated GABAergic input compared to their adjacent Control PCs, this (KL OX) relative increase in inhibitory drive was not beyond the inhibition recorded in PCs from separate Sham animals (**Figure 4F**). That is, the focal gain in synaptic input to KL OX PCs appears to come at the expense of decreasing input to nearby Control PCs. Thus, KL-Kit levels may not set the number of MLI:PC release sites, but may instead influence the proportion of synapses that are functional for neurotransmission (**Figure 4G**). Such a requirement is consistent with the impaired synaptic function observed under both widespread conditional knockout and sparse viral manipulation.

## Discussion

For genes essential to survival or reproduction, germline knockout strategies are not feasible for evaluating postnatal physiology. Among such genes, Kit is an example of a highly pleiotropic gene, and so the interpretation of global hypomorphs is challenging and the recombination of conditional alleles outside of desired tissues can lead to lethal or sterile phenotypes. By generating a conditional knockout mouse, we were able to produce viable animals with Kit depleted from the cerebellum to reveal a role in synapse function.

MLI number, distribution, action potential firing, and the density of GABAergic synaptic puncta upon PCs, are all normal in MLI Kit KO. These data suggest that while MLI axon terminals are present in Kit KO (perhaps related to the smaller size of synaptic puncta and pinceaux), they may be less functionally mature. An increased failure rate between action potential generation and neurotransmitter release would be consistent with the normal firing rate and VGAT puncta density but decreased sIPSC and mIPSC frequency observed. Under the PPR paradigm, the apparent equivalent evoked responses may be due to direct stimulation of axon terminals and/or recruitment of multiple MLIs.

Kit KO most directly impacts the MLI:PC synapse, based upon normal miniature events for PF/CF:PC (mEPSC in PC) and MLI:MLI (mIPSC in MLI) synapses. This is perhaps expected given the cell type specific expression of KL by PCs and Kit by MLIs, however, it is a critical distinction as Cerebellins[41] and Calsystenin[42] impact multiple forms of synaptic input to PCs. It will be informative to determine if the residual inhibitory drive to PCs observed in MLI Kit KO or PC KL KO comes from PC axon collaterals[43-46] whose input we might expect to be preserved if KL-Kit functions primarily to mediate connectivity between different cell types.

Our results demonstrate that the KL-Kit axis, from embryonic development through young adulthood (P56), can alter GABAergic drive to PCs. These results suggest that KL-Kit may be necessary to maintain, and perhaps capable of modulating, connectivity in the adult cerebellum. As each MLI (e.g. basket cell) may have axon collaterals that target multiple PCs, and as each PC may receive input from multiple MLIs, it is interesting to speculate that dynamics in the expression or shedding of KL may act through presynaptic Kit to tune the degree of convergent MLI:PC inhibitory drive. This would complement existing forms of modulation at the MLI:PC synapse, such those dependent upon other PC derived signaling molecules, like endocannabinoids[47-49] or peptides like secretin[50,51] and CR [52]. The physiology of PCs, and the structure of MLI:PC inhibition, also varies over zones such as those identified by Zebrin-II and PLC β4[53-57]; whether there is anatomical variation in KL or Kit expression, signaling, or dependency, remains to be determined.

Kit is a receptor tyrosine kinase that can activate multiple downstream effectors including Src family kinases, PLC, PI3K/mTOR, and the MAPK pathway, the latter two notable for their shared affiliation with synapse phenotypes and autism spectrum disorder. Furthermore, trans-cellular interactions between KL and Kit may function in a kinase-independent cell adhesion molecule modality[58,59]. There is a substantial literature illustrating the importance of adhesion molecules in the organization and maintenance of MLI:PC inhibition, such as neurexins/neuroligins, dystrophin/dystroglycan, semaphorins, and neurofascins[41,42,60-64]. Much of what is understood about the maintenance of PC inhibition is revealed by post-synaptic phenotypes; that is, cis-and trans interacting proteins that, via gephyrin, maintain the organization of PC $GABA_A$ receptors. It is notable therefore that MLI Kit or PC KL KO have a more predominant effect on mIPSC frequency than on amplitude, suggesting a presynaptic phenotype. A compatible model is that PC derived KL may act retrograde/trans-synaptic to modulate MLI axon function via Kit binding/activity.

Despite the reduced PC inhibition resulting from MLI Kit KO or from PC KL KO, we have not observed overt cerebellar signs (i.e., ataxia). We suspect that this is due to compensation. Even the developmental ablation of functional $GABA_A$ channels in PCs does not produce overt motor signs, while adulthood ablation ca [65]. Thus, we might unmask behavioral phenotypes if KL or Kit KO is delayed. Beyond direct inhibition of PCs, MLI inhibition constrains granule cell mediated PC dendritic excitation and thus gates the conversion of PC LTD to LTP at the PF-PC synapse in motor learning[66,67]. It is therefore possible that KL or Kit KO may only reveal phenotypes in motor learning (or other cerebellar-plasticity dependent) behaviors. Not inconsistent with a role in learning, global hypomorphs for KL or Kit have altered hippocampal neurophysiology and Water Maze performance[68-70]. Continuous expression of KL and Kit in specific neurons may thus ultimately reflect not only a role in development or maintenance of synaptic function as suggested here, but also in plastic modulation of synaptic strength.

Despite the importance of future works to determine molecular mechanisms and organismal consequences, our study is a discrete advance because it establishes that KL-Kit regulate mammalian central synapse function. Here, we demonstrate impacts at the mouse GABAergic MLI:PC synapse; however, Kit and KL exist in diverse organisms and neuronal populations including glutamatergic neurons of the hippocampus, and neurons in olfactory bulb, basal forebrain, and brainstem. It is therefore feasible that the synaptic phenotypes reported here reflect that KL-Kit is broadly capable of influencing connectivity.

## Main Figure Legends

**Figure 1:** Design and validation of a Kit conditional knockout mouse.

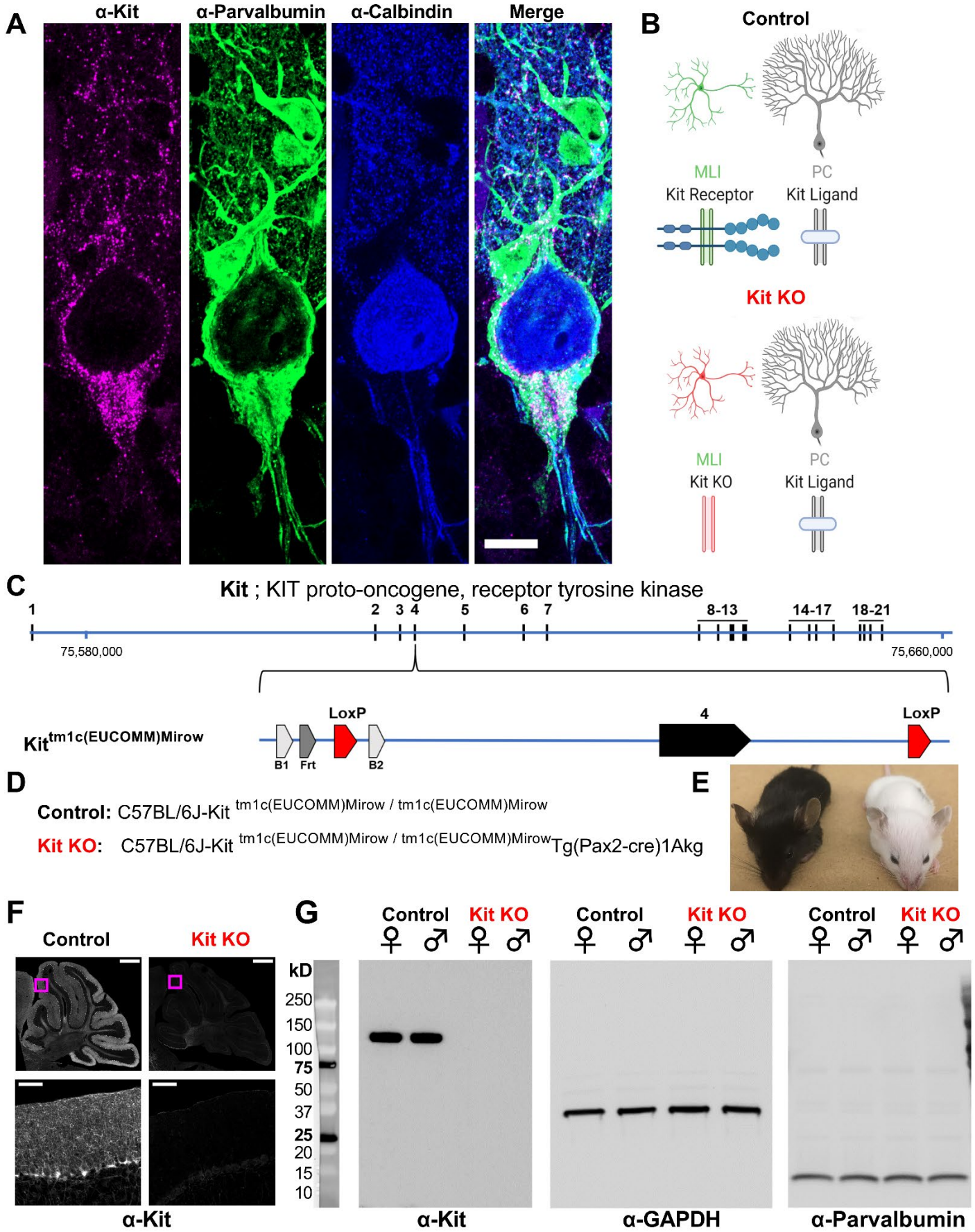

**Figure 1, Continued**

(A,B) Kit receptor tyrosine kinase (Kit) is enriched in parvalbumin positive GABAergic interneurons of the molecular layer (i.e. basket and stellate cells, MLIs) of the cerebellar cortex, where they synapse upon each other and upon Purkinje cells (PCs, Calbindin+), which express Kit Ligand (KL). Scale bar 10 microns. Expression pattern schematized in B.

(C) In humans and mice, Kit is encoded by up to 21 exons, which in mouse is encoded on the plus strand of chromosome 5 at 75,735,647-75,817,382 bp. We generated a Kit conditional knockout mouse in which Kit Exon 4 is flanked by LoxP sites.

(D) We generated Control mice homozygous for the Kit floxed allele $Kit^{tm1c(EUCOMM)Mirow}$ which varied in Pax2-Cre)1Akg transgene status, with the goal of depleting Kit from MLIs in embryonic development.

(E) Male and Female, Control and Kit KO mice were born in equal ratios. KO mice were notably hypopigmented in hair and whiskers, though not eyes.

(F) Confocal microscopy of Kit immunoreactivity in age and sex matched Control and Kit KO littermates demonstrates the established enrichment of Kit in the molecular layer of the cerebellar cortex, and its loss in Kit KO. Scale Bar 500 microns top row, 50 microns inset.

(G) Utilizing a distinct assay and primary antibody, we confirm the detection of Kit immunoreactivity in Controls, and its loss in Kit KO litter mates of either sex by Western Blot of total protein lysates of cerebella. We affirmed equivalent protein loading by GAPDH and parvalbumin.

**Figure 2 :**The knockout of Kit from Cerebellar Cortex Interneurons Impairs Inhibition of Purkinje Cells.

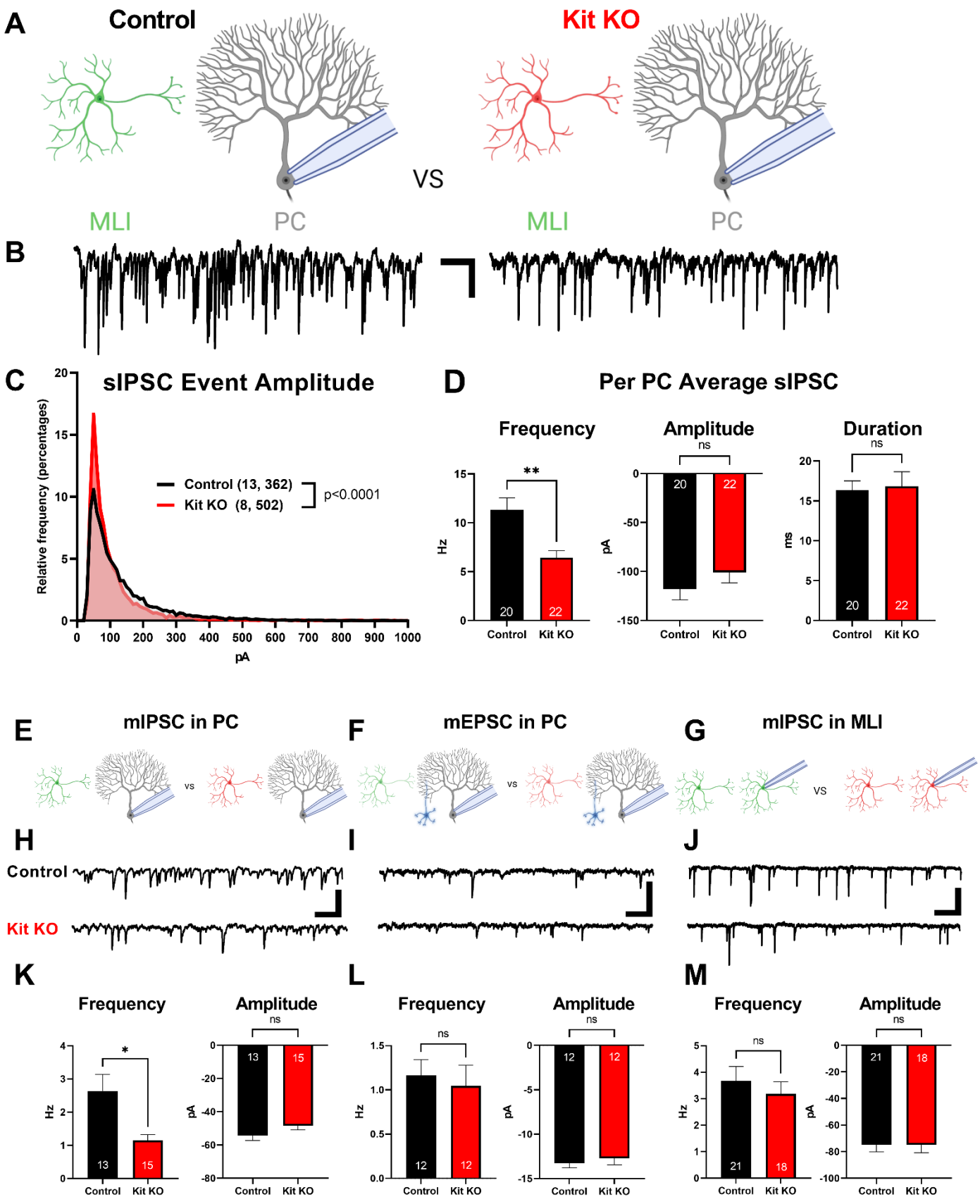

**Figure 2, Continued**

(A,B) Experimental design and example traces of postsynaptic currents in Purkinje Cells (PCs) from Control animals or from those with Kit KO from cerebellar cortex molecular layer interneurons (MLIs). Scale bar is 500 ms x 100 pA.

(C) A frequency distribution plot for individual sIPSC event amplitudes recorded in PCs as in A,B. A KS test reveals a significant difference in the distribution of these event amplitudes; $p<0.0001$, n in chart.

(D) For each PC, the average Frequency, Amplitude, and Duration of sIPSC was determined. There was a ~50% decrease in sIPSC frequency $p=0.0013$, but no change in Amplitude or Duration.

(E-G) Experimental design: In separate experiments, we recorded miniature postsynaptic currents from PCs or from MLIs in Control and in Kit KO animals.

(H) Example traces of mIPSCs or (I) mEPSCs recorded in PCs, and example traces of mIPSC in MLIs, all from Control or from Kit KO animals. Scale for H and J is 50 pA, 25 pA for I, all 500 ms.

(K-M) Analysis of per cell average miniature event Frequency and Amplitude revealed that Kit KO reduced mIPSC frequency, but not amplitude, in PCs by >50%, $p=0.013$. mEPSCs in PCs and mIPSC in MLIs were not different between Control and Kit KO.

N in charts, refers to number of cells. Error bars are SEM. Statistical significance is by two-tailed t-test, with Welch's correction as needed. NS indicates $p\geq0.05$.

**Figure 3:** Knockout of Kit Ligand from Purkinje Cells decreases their inhibitory input.

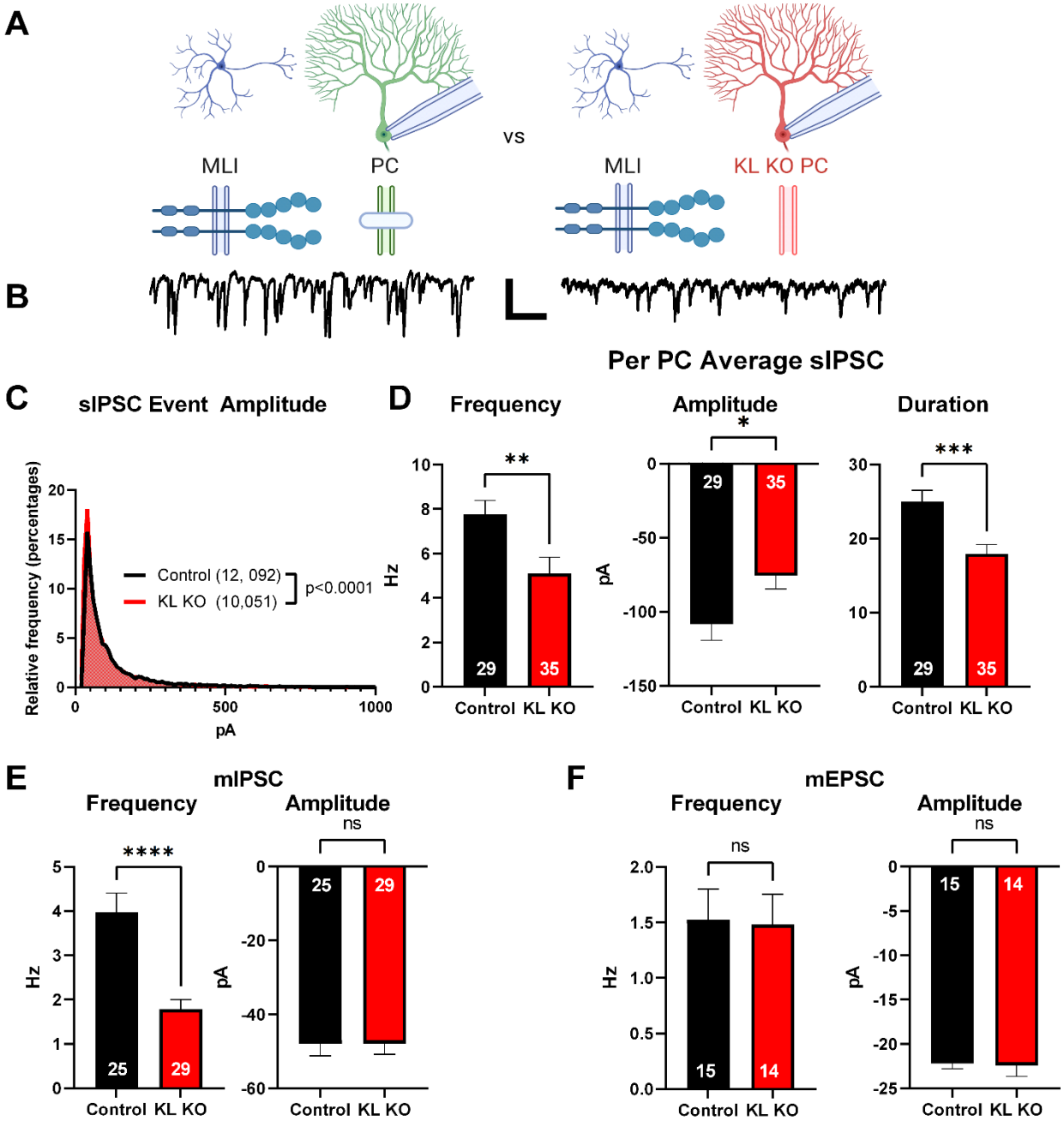


(A,B) Experimental design and example traces of inhibitory postsynaptic currents detected in Purkinje Cells (PCs) from Control animals or from those with Kit Ligand knockout (KL KO) accomplished by a PCP2-Cre x KL Floxed strategy. Scale bar is 500 ms x 100 pA.

C) A frequency distribution plot for individual sIPSC event amplitudes recorded in PCs as in A,B. A KS test reveals a significant difference in the distribution of these event amplitudes; p<0.0001, n in chart.

(D) For each PC, the average Frequency, Amplitude, and Duration of sIPSC was determined. There was a ~30-40%% decrease in sIPSC Frequency p=0.0078, Amplitude p=0.024 and Duration p=0.0006.

(E, F) The average mIPSC recorded in PC KL KO vs Control PCs had a >50% decreased Frequency p<0.0001 without a corresponding decrease in mIPSC Amplitude. The average mEPSC Frequency and Amplitude recorded in separate PCs did not differ between Control and KL KO.

N in charts, refers to number of cells. Error bars are SEM. Statistical significance is by two-tailed t-test, with Welch's correction as needed. NS indicates p>=0.05.

**Figure 4** Local levels of Kit Ligand influence the inhibition Purkinje cells receive.

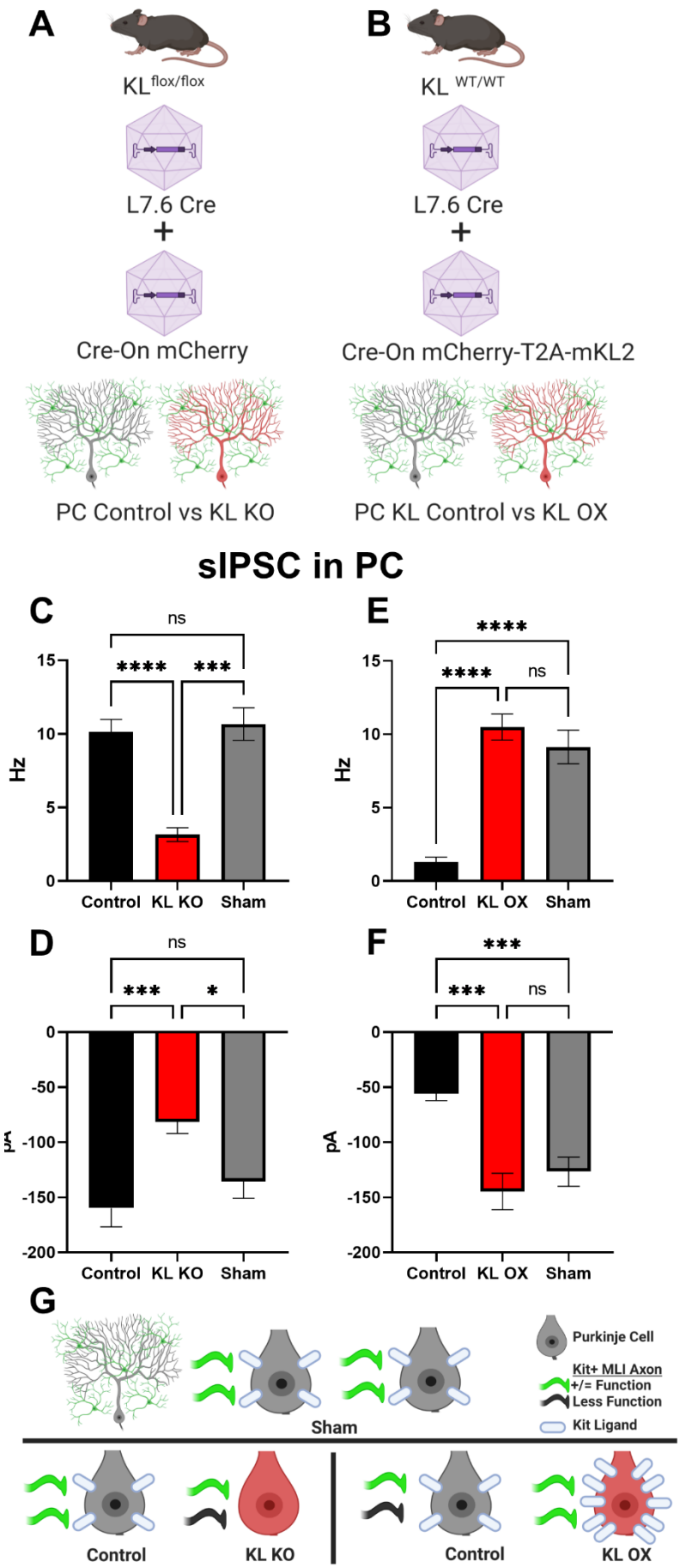


(A) To accomplish *in vivo* mixtures of Control and Kit Ligand knockout (KL KO) Purkinje Cells (PCs), an AAV encoding Cre under the PC specific L7.6 promoter was co-injected with an AAV encoding a Cre-On mCherry cassette under the Ef1α promoter.

(B) To accomplish *in vivo* mixed population of Control and Kit Ligand overexpressing (KL OX) PCs, the L7.6 Cre AAV was co-injected with AAV expressing mCherry and (T2A) murine Kit Ligand isoform 2 under the Ef1α promoter.

(C,D) In animals injected at P18, PC KL KO neurons demonstrated a ~70% decrease in sIPSC event frequency compared to adjacent Control PCs ($p<0.0001$) or PCs recorded from Sham control animals ($p=0.0002$). Control vs Sham sIPSC frequency was not significantly different. Similarly, the sIPSC event amplitude was significantly reduced by PC KL KO vs adjacent Control PCs ($p=0.0009$) or those from Sham animals ($p=0.31$). Control vs Sham sIPSC amplitude was not different.

(E, F) In animals injected at P18, PC KL OX neurons demonstrated an 8-fold increase in sIPSC Frequency vs local Control PCs ($p<0.0001$). The frequency of sIPSC events in KL OX PCs was not significantly different from PCs recorded in different Sham animals; this Sham PC sIPSC frequency (while comparable across studies) was 7-fold higher than Control PCs within the KL OX experimental animals ($p<0.0001$). A similar pattern was found for sIPSC amplitude, being significantly elevated (3-fold) in the KL OX PCs vs their neighboring Control PCs ($p=0.0003$), but not distinguishable from those recorded in Sham animals.

(G) Proposed model for a function of Purkinje Cell Kit Ligand and Molecular Layer Interneuron Kit. Under normal conditions, the balanced expression of PC KL mediates equivalent presynaptic function of MLI axons via Kit. In focal PC KL KO or PC KL OX, those PCs with the locally highest KL levels sustain nominal levels of MLI mediated inhibition at the expense of reduced functional input to out-competed PCs.

N in charts, refers to number of cells. Error bars are SEM. Statistical significance is by Brown-Forsythe ANOVA test with Dunnett's T3 multiple comparisons test. NS indicates $p>=0.05$.

**Supplementary Information**

**Five Figures and Associated Legends**

**Figure S1:** Kit receptor tyrosine kinase is a highly conserved gene affiliated with neurological impairment.

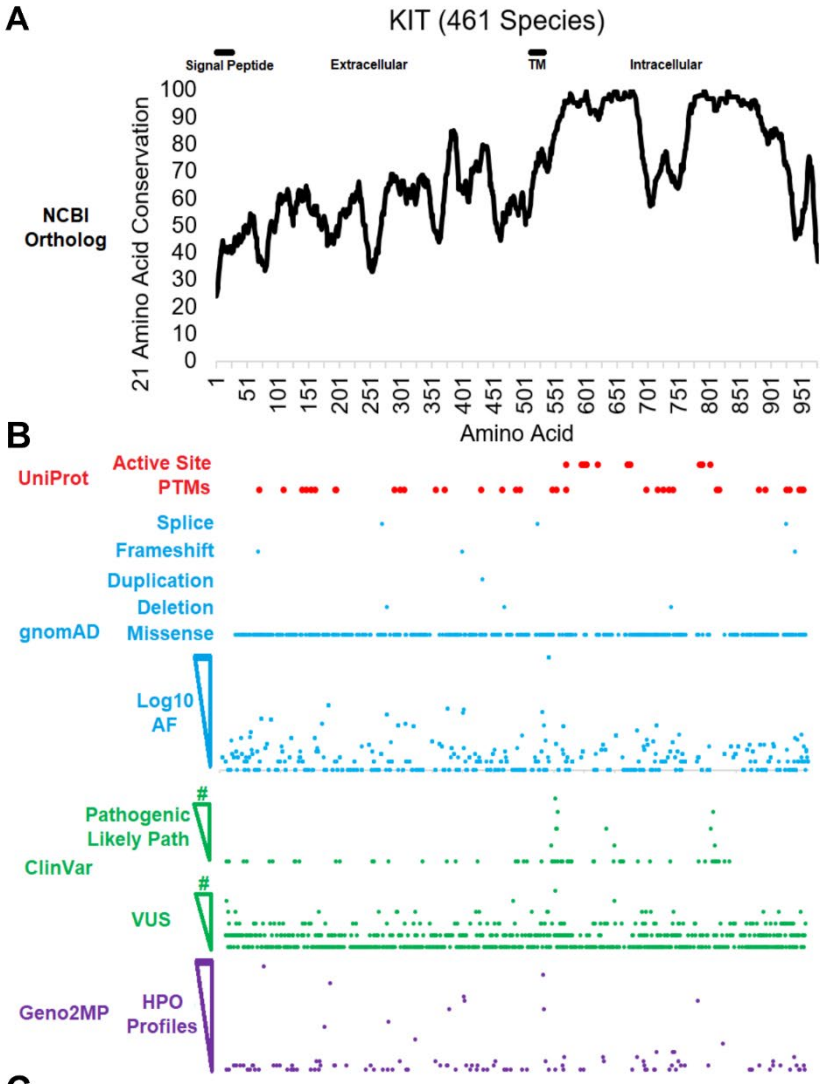


C

| hgvsCndaVar | hgvsProteinVar | Annotation | AA | Conservation 461 Species | CADD score | Polyphen2 | gnomAD Allele Count | HPO Profiles | w/ Nervous System Abnormality |
|---|---|---|---|---|---|---|---|---|---|
| c.2836C>T | p.(R946*) | Nonsense | - | - | 39 | unknown | 3.99E-05 | 4 | 4 |
| c.1694G>T | p.(G565V) | missense | 565 | 99.56616052 | 29.1 | probably | 1.83E-04 | 4 | 1 |
| c.316T>G | p.(S106A) | missense | 106 | 95.01084599 | 23.6 | probably | 0 | 1 | 1 |
| c.340C>G | p.(P114A) | missense | 114 | 92.40780911 | 22.4 | probably | 8.01E-06 | 2 | 1 |
| c.464C>T | p.(P155L) | missense | 155 | 54.44685466 | 24.6 | possibly | 3.98E-05 | 2 | 1 |
| c.821C>T | p.(T274M) | missense | 274 | 68.54663774 | 18.17 | possibly | 4.90E-04 | 12 | 2 |
| c.910A>G | p.(T304A) | missense | 304 | 67.02819957 | 18.1 | probably | 2.07E-04 | 1 | 1 |
| c.1344G>C | p.(Q448H) | missense | 448 | 65.29284165 | 15.9 | probably | 1.59E-05 | 2 | 1 |
| c.1689A>G | p.(I563M) | missense | 563 | 95.87852495 | 18.37 | possibly | 0 | 1 | 1 |
| c.1889A>G | p.(H630R) | missense | 630 | 99.56616052 | 24.4 | probably | 3.18E-05 | 4 | 1 |
| c.2057G>A | p.(R686H) | missense | 686 | 99.13232104 | 19.18 | probably | 3.19E-05 | 1 | 1 |
| c.2096A>G | p.(E699G) | missense | 699 | 55.96529284 | 17.08 | possibly | 0 | 1 | 1 |
| c.2411G>A | p.(R804Q) | missense | 804 | 97.61388286 | 32 | probably | 1.19E-05 | 1 | 1 |
| c.2732C>A | p.(P911H) | missense | 911 | 97.8308026 | 27.2 | probably | 2.79E-05 | 3 | 1 |
| c.2771T>C | p.(I924T) | missense | 924 | 94.36008677 | 15.63 | possibly | 4.65E-05 | 2 | 1 |
| c.2863G>T | p.(V955L) | missense | 955 | 67.02819957 | 15.54 | possibly | 1.55E-05 | 1 | 3 |

(A) KIT protein sequences were extracted from NCBI ortholog on March 2023 and aligned with MUSCLE. Conservation was placed on a 21 amino acid sliding window to calculate linear motifs, as done in PMID:3557896. The intracellular domain possesses a split cytoplasmic kinase motif demonstrating high conservation across 461 species.

(B) Alignment of Active Site and Post-Translational Motif (PTMs) to Kit amino acid conservation and gnomAD, ClinVar, and Geno2MP human variants.

(C) Human Genome Variation Society annotations for human DNA and corresponding encoded amino acid changes affiliated with their mutational class (Annotation), Site (AA), and Conservation across 461 species. Combined Annotation Dependent Depletion (CADD) score for deleteriousness of SNV or indel variants. Polymorphism Phenotyping v2 (PolyPhen2) annotations predict impact of amino acid substitution on Kit structure function. Allele counts in Gnomad and the number of profiles in the Human Phenotype Ontology associated with Nervous System Abnormality.

**Figure S2**: Kit knockout does not alter molecular layer interneuron number or distribution.

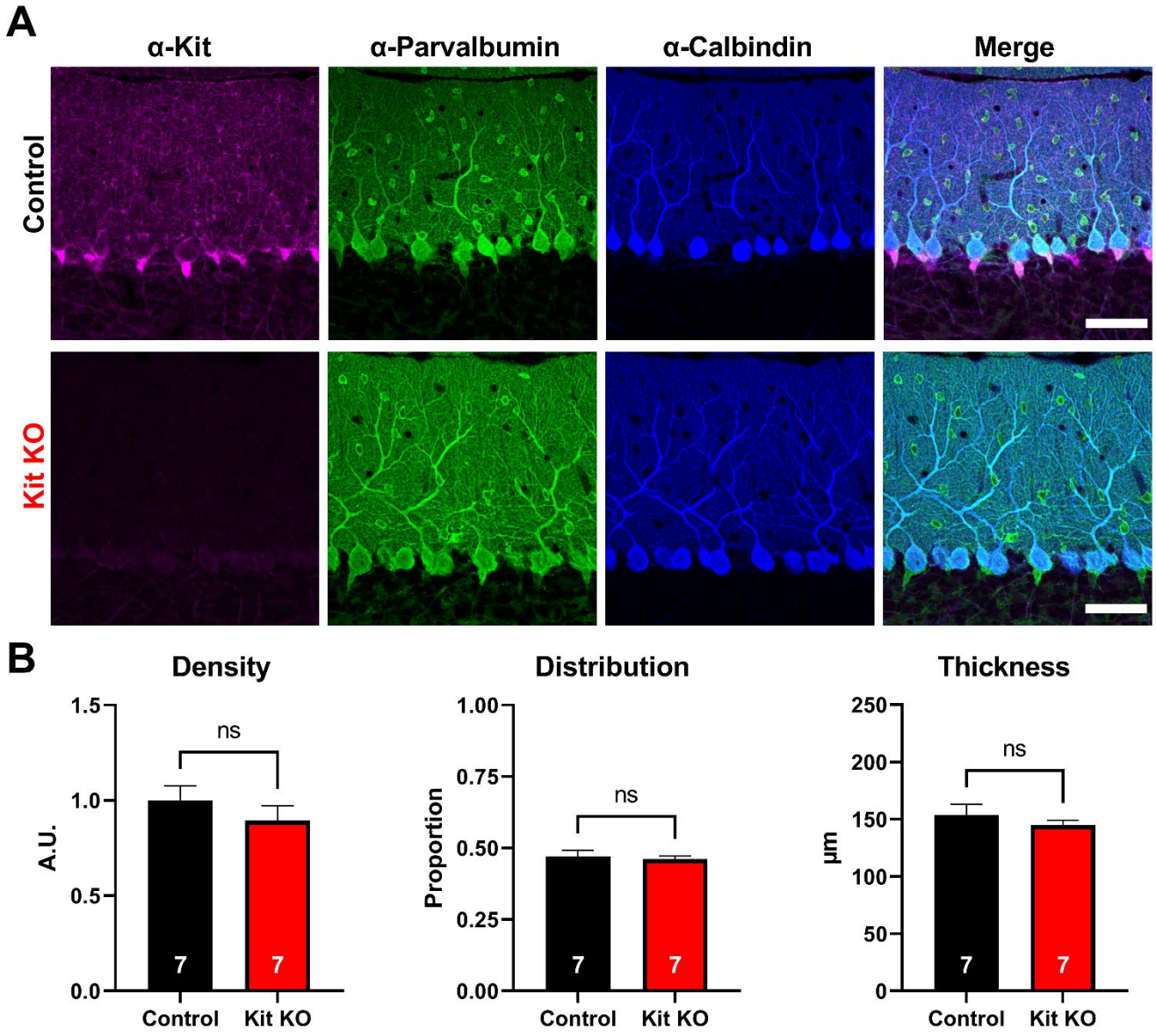


(**A**) Immunohistochemistry and confocal microscopy of Control and Kit KO mouse cerebellar cortex validates the normal enrichment and targeted depletion of Kit in Control and Kit KO animals respectively. Parvalbumin immunoreactivity labels Molecular Layer Interneurons and Purkinje Cells, which are also selectively labeled by Calbindin immunoreactivity.

(**B**) Quantification of the density of Parvalbumin positive and or Calbindin negative somas within the molecular layer reveals that the Density of MLIs is not reduced by Kit KO. Quantification of the average position of MLI somas between the basal (0) and distal (1) borders of the Molecular Layer reveals that the Control and Kit KO MLIs have comparable distributions within the molecular layer. Quantification of the thickness of the the molecular layer reveals no significant difference between Control and Kit KO conditions.

Statistical significance was evaluated by two-tailed t-test with Welch's correction as necessary, except for Distribution which utilized Mann-Whitney. N in columns reveals the number of different animals whose comparable tissues were evaluated. NS reflects a p value >0.05.

**Figure S3**: Kit knockout does not alter intrinsic properties of molecular layer interneurons.

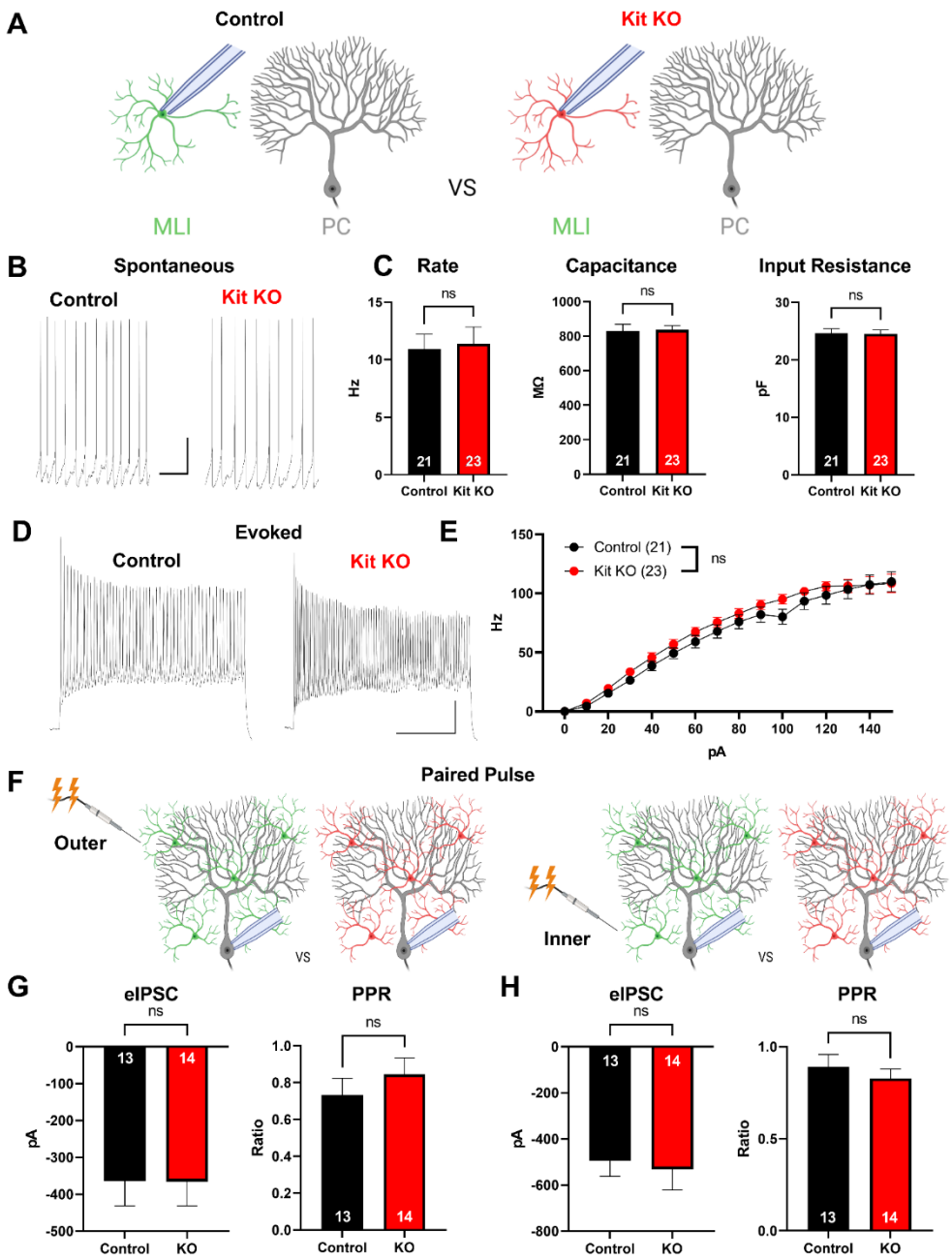


(**A**) Experimental design. Patch clamp recordings were performed on Molecular Layer Interneurons in acute cerebellar slice preparations from Control or from Kit KO animals.

(**B,C**) Patch clamp recordings of spontaneous action potentials and intrinsic properties in Control and Kit KO MLIs revealed no significant difference in firing Rate, or in membrane Capacitance or Input Resistance. Scale bar 100 ms x 10mV.

(**D, E**) Current steps were injected into Control or Kit KO MLIs, Example traces (D) and quantification (E) revealed no significant effect of genotype on firing rate. Scale bar 100 ms x 10mV.

(**F**) Experimental Design. Paired pulses were delivered via stimulating electrode placed in the Outer or the Inner molecular layer, and evoked Inhibitory Post Synaptic Currents were evaluated.

(**G, H**) The average strength of the first evoked response, nor the Paired Pulse Ratio, did not differ between Control and Kit KO, under either stimulation of the Outer or Inner molecular layer.

Statistical significance was evaluated by two-tailed t-test with Welch's correction as necessary. N in columns reveals the number of different recorded cells per condition. NS reflects a p value >0.05.

**Figure S4**: Kit knockout reduces the size of molecular layer interneuron synaptic structures.

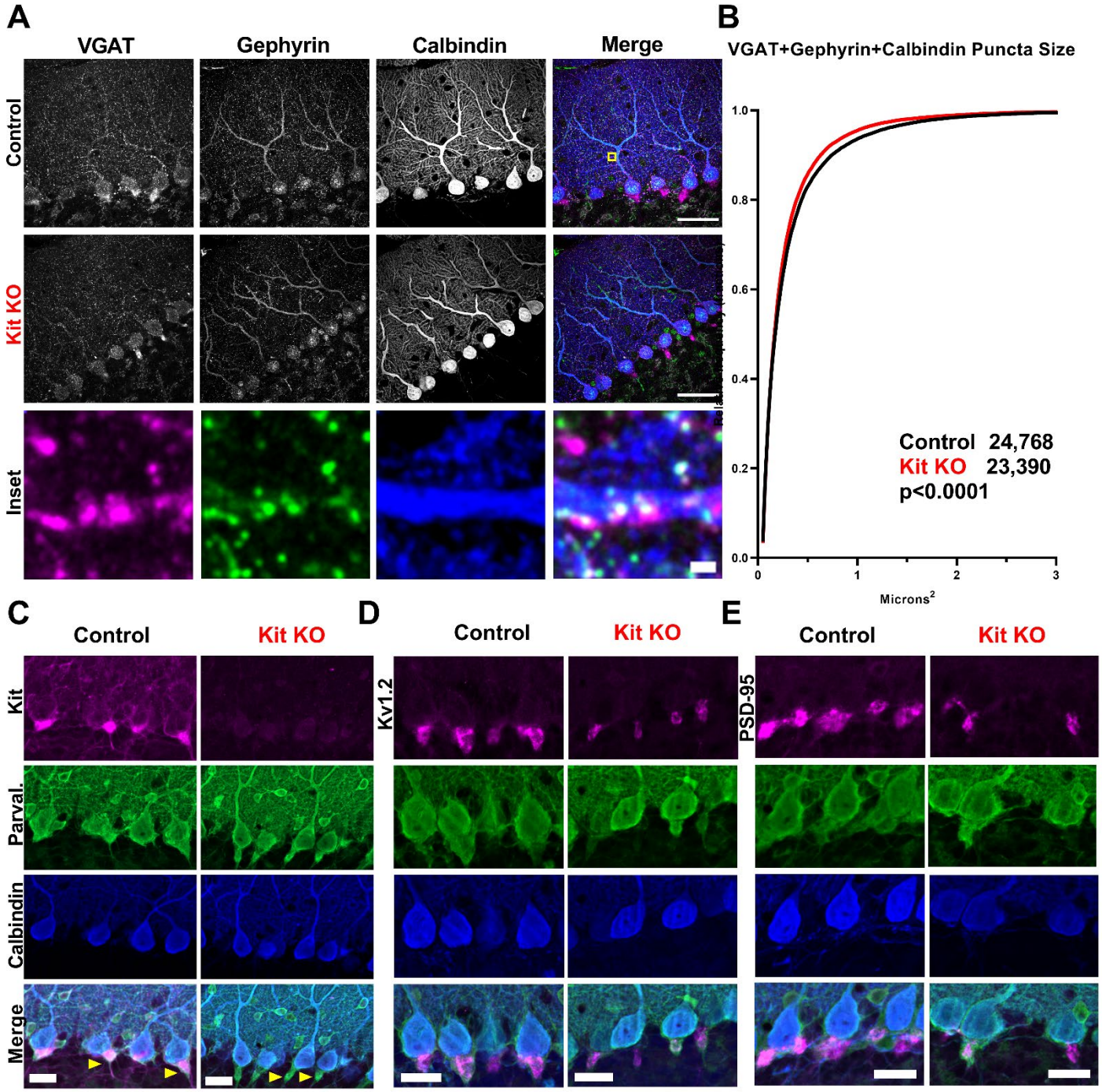


(**A**) Immunohistohemistry and confocal microscopy of presynaptic (VGAT) and postsynaptic (Gephyrin) markers of GABAErgic synapses upon Purkinje Cells (Calbindin), for both Control and Kit KO. An Inset from Control (Yellow Box, first Row Merge ROI), demonstrates example triple positive puncta. First two rows, scale bar 50 microns.

(**B**) In data not shown, the density of GABAergic synaptic puncta upon Purkinje Cells was not impacted by Kit KO, however, a KS test of the distribution of the sizes of individual puncta from Control vs Kit KO revealed a significant ($P<0.0001$) decrease. N in chart reflects number of puncta analyzed from 7 Control and from 7 Kit KO animals.

(**C, D, E**) Immunohistochemistry and confocal microscopy of markers of the pinceau formation of MLI axons upon PC soma and initial axon segments. For both Control and Kit KO, Calbindin and Parvalbumin immunoreactivity was determined in conjunction with pinceau markers Kit, Kv1.2, or PSD-95. As evidence by Parvalbumin positive calbindin negative pinceaux structures in Kit KO in C, pinceaux structures still exist in Kit KO, though appear smaller. This was affirmed by reduced area of Kv1.2 immunoreactivity, and by POSD-95 immuno-reactivity. Scale bars are 50 microns.

**Figure S5**: Sparse Acute Depletion of Kit Ligand Reduces GABAergic Input To Purkinje Cells.

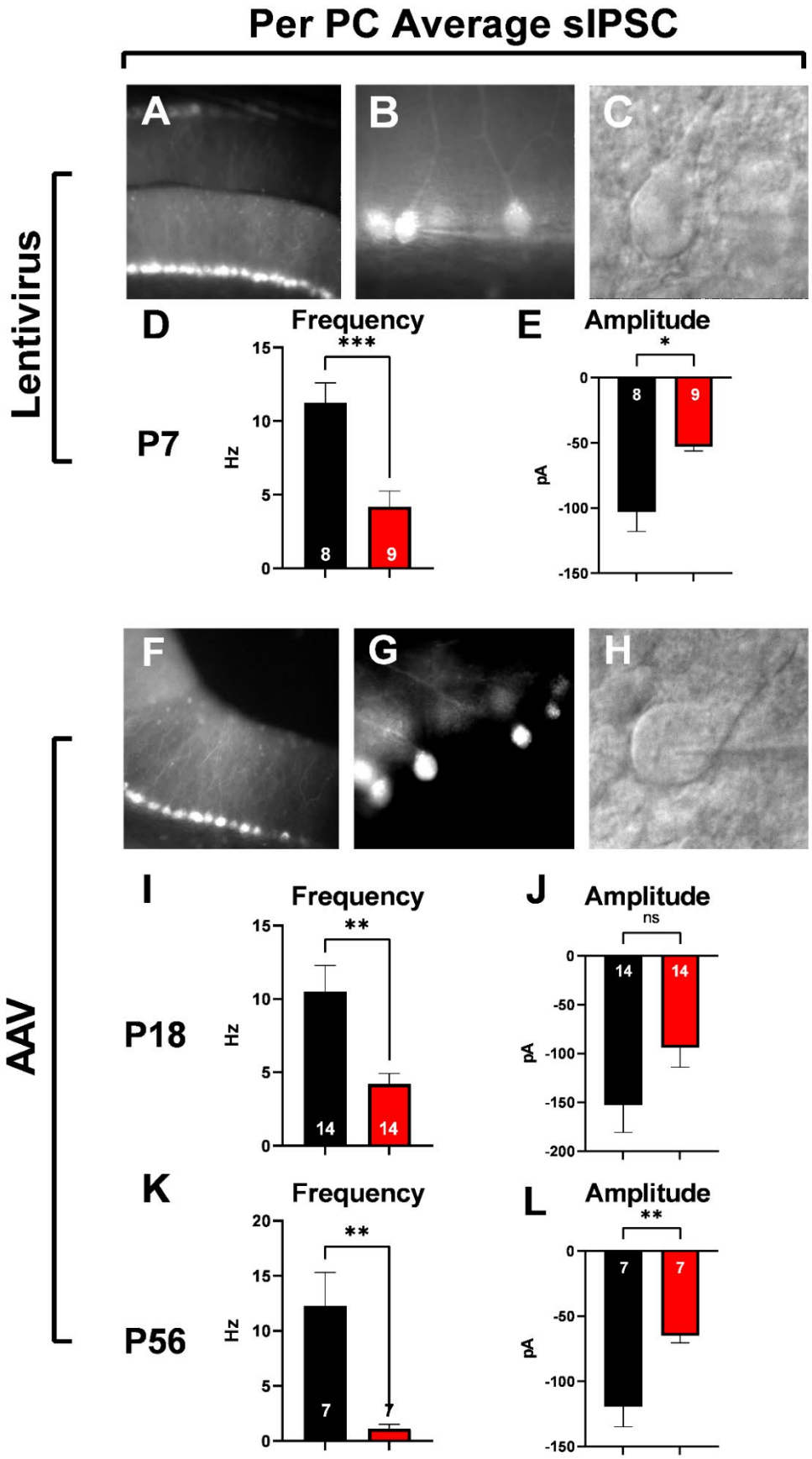


**(A, B, C**) Lentivirus encoding mCherry-T2A-Cre under the Purkinje Cells specific promoter L7.6 was injected into postnatal day 7 mice homozygous for a Kit Ligand (KL) floxed allele at P7. Demonstrated here is an area of direct hit and high transduction. (B) Areas with sparse PC transduction were used to record from KL KO or from uninfected adjacent Control PCs, with an example of a IR-DIC identified PC (C).

(**D, E**). Quantification of the average sIPSCs recorded from P7 Control or sparse KL KO PCs revealed that KL KO reduced both the frequency (p=0.0008) and the amplitude (p=0.012) of GABAergic inhibition of PCs by ~50%.

(**F, G, H**) AAV encoding Cre under the L7.6 promoter was co-injected with an AAV encoding Cre-On mCherry under the Ef1α promoter into the cerebellum of postnatal day 18 or 56 KL floxed homozygous mice. Demonstrated in F is a direct hit with high transduction, areas as in (G) with sparse transduction were selected for recordings of mCherry positive KL KO PCs and their adjacent uninfected Control PCs patched under IR-DIC (H).

**(I,J,K, L**). Analysis of the average sIPSC Frequency and Amplitude in Control and KL KO PCs revealed that at either P18 (p=0.005) or P56 (p=0.008), KL KO robustly reduced GABAergic event frequency in PCs by over 50%. The reduction in sIPSC amplitude reached significance in the P56 (p=0.0096), but not the P18 cohort, here (p=0.104).

Statistical significance was evaluated by two-tailed t-test with Welch's correction as necessary. N in columns reveals the number of different cells recorded. NS reflects a p value >0.05.

## References


1. Chen, S., Francioli, L.C., Goodrich, J.K., Collins, R.L., Kanai, M., Wang, Q., Alföldi, J., Watts, N.A., Vittal, C., Gauthier, L.D., et al. (2022). A genome-wide mutational constraint map quantified from variation in 76,156 human genomes. bioRxiv, 2022.2003.2020.485034. 10.1101/2022.03.20.485034.

2. Bernstein, A., Chabot, B., Dubreuil, P., Reith, A., Nocka, K., Majumder, S., Ray, P., and Besmer, P. (1990). The mouse W/c-kit locus. Ciba Found Symp *148*, 158-166; discussion 166-172.

3. Yarden, Y., Kuang, W.J., Yang-Feng, T., Coussens, L., Munemitsu, S., Dull, T.J., Chen, E., Schlessinger, J., Francke, U., and Ullrich, A. (1987). Human proto-oncogene c-kit: a new cell surface receptor tyrosine kinase for an unidentified ligand. EMBO J *6*, 3341-3351.

4. Lennartsson, J., and Ronnstrand, L. (2012). Stem cell factor receptor/c-Kit: from basic science to clinical implications. Physiol Rev *92*, 1619-1649. 10.1152/physrev.00046.2011.

5. Keshet, E., Lyman, S.D., Williams, D.E., Anderson, D.M., Jenkins, N.A., Copeland, N.G., and Parada, L.F. (1991). Embryonic RNA expression patterns of the c-kit receptor and its cognate ligand suggest multiple functional roles in mouse development. EMBO J *10*, 2425-2435.

6. Motro, B., van der Kooy, D., Rossant, J., Reith, A., and Bernstein, A. (1991). Contiguous patterns of c-kit and steel expression: analysis of mutations at the W and Sl loci. Development *113*, 1207-1221.

7. Hirota, S., Ito, A., Morii, E., Wanaka, A., Tohyama, M., Kitamura, Y., and Nomura, S. (1992). Localization of mRNA for c-kit receptor and its ligand in the brain of adult rats: an analysis using in situ hybridization histochemistry. Brain Res Mol Brain Res *15*, 47-54. 10.1016/0169-328x(92)90150-a.

8. Manova, K., Bachvarova, R.F., Huang, E.J., Sanchez, S., Pronovost, S.M., Velazquez, E., McGuire, B., and Besmer, P. (1992). c-kit receptor and ligand expression in postnatal development of the mouse cerebellum suggests a function for c-kit in inhibitory interneurons. J Neurosci *12*, 4663-4676.

9. Telfer, M.A., Sugar, M., Jaeger, E.A., and Mulcahy, J. (1971). Dominant piebald trait (white forelock and leukoderma) with neurological impairment. Am J Hum Genet *23*, 383-389.

10. Finucane, B., Scott, C.I., Jr., and Kurtz, M.B. (1991). Concurrence of dominant piebald trait and fragile X syndrome. Am J Hum Genet *48*, 815.

11. Funderburk, S.J., and Crandall, B.F. (1974). Dominant piebald trait in a retarded child with a reciprocal translocation and small intercalary deletion. Am J Hum Genet *26*, 715-722.

12. Lacassie, Y., Thurmon, T.F., Tracy, M.C., and Pelias, M.Z. (1977). Piebald trait in a retarded child with interstitial deletion of chromosome 4. Am J Hum Genet *29*, 641-642.

13. Kilsby, A.J., Cruwys, M., Kukendrajah, C., Russell-Eggitt, I., Raglan, E., Rajput, K., Lohse, P., and Brady, A.F. (2013). Homozygosity for piebaldism with a proven KIT mutation resulting in depigmentation of the skin and hair, deafness, developmental delay and autism spectrum disorder. Clin Dysmorphol *22*, 64-67. 10.1097/MCD.0b013e32835e8ce5.

14. Gore, B.B., Wong, K.G., and Tessier-Lavigne, M. (2008). Stem cell factor functions as an outgrowth-promoting factor to enable axon exit from the midline intermediate target. Neuron *57*, 501-510. 10.1016/j.neuron.2008.01.006.

15. Su, Y., Cui, L., Piao, C., Li, B., and Zhao, L.R. (2013). The effects of hematopoietic growth factors on neurite outgrowth. PLoS One *8*, e75562. 10.1371/journal.pone.0075562.

16. Guijarro, P., Wang, Y., Ying, Y., Yao, Y., Jieyi, X., and Yuan, X. (2013). In vivo knockdown of cKit impairs neuronal migration and axonal extension in the cerebral cortex. Dev Neurobiol *73*, 871-887. 10.1002/dneu.22107.

17. Mashayekhi, F., and Gholizadeh, L. (2011). Administration of anti-c-kit antibody into the cerebrospinal fluid leads to increased cell death in the developing cerebral cortex. Saudi J Biol Sci *18*, 261-266. 10.1016/j.sjbs.2011.01.006.

18. Aoki, H., Hara, A., and Kunisada, T. (2017). Induced haploinsufficiency of Kit receptor tyrosine kinase impairs brain development. JCI Insight *2*. 10.1172/jci.insight.94385.

19. Kim, D., Im, J.O., Won, Y.J., Yoon, S.Y., Lee, E.J., Lee, J.H., and Hong, H.N. (2003). Upregulation of c-Kit receptor and stem cell factor in cerebellar inhibitory synapses in response to kainic acid. J Neurosci Res *71*, 72-78. 10.1002/jnr.10466.

20. Skarnes, W.C., Rosen, B., West, A.P., Koutsourakis, M., Bushell, W., Iyer, V., Mujica, A.O., Thomas, M., Harrow, J., Cox, T., et al. (2011). A conditional knockout resource for the genome-wide study of mouse gene function. Nature *474*, 337-342. 10.1038/nature10163.

21. Ohyama, T., and Groves, A.K. (2004). Generation of Pax2-Cre mice by modification of a Pax2 bacterial artificial chromosome. Genesis *38*, 195-199. 10.1002/gene.20017.

22. Heintz, N. (2004). Gene expression nervous system atlas (GENSAT). Nat Neurosci *7*, 483. 10.1038/nn0504-483.

23. Ding, L., Saunders, T.L., Enikolopov, G., and Morrison, S.J. (2012). Endothelial and perivascular cells maintain haematopoietic stem cells. Nature *481*, 457-462. 10.1038/nature10783.

24. Barski, J.J., Dethleffsen, K., and Meyer, M. (2000). Cre recombinase expression in cerebellar Purkinje cells. Genesis *28*, 93-98.

25. Fricano-Kugler, C.J., Williams, M.R., Salinaro, J.R., Li, M., and Luikart, B. (2016). Designing, Packaging, and Delivery of High Titer CRISPR Retro and Lentiviruses via Stereotaxic Injection. J Vis Exp. 10.3791/53783.

26. Luikart, B.W., Schnell, E., Washburn, E.K., Bensen, A.L., Tovar, K.R., and Westbrook, G.L. (2011). Pten knockdown in vivo increases excitatory drive onto dentate granule cells. J Neurosci *31*, 4345-4354. 10.1523/JNEUROSCI.0061-11.2011.

27. Williams, M.R., DeSpenza, T., Jr., Li, M., Gulledge, A.T., and Luikart, B.W. (2015). Hyperactivity of newborn Pten knock-out neurons results from increased excitatory synaptic drive. J Neurosci *35*, 943-959. 10.1523/JNEUROSCI.3144-14.2015.

28. Martin, F.H., Suggs, S.V., Langley, K.E., Lu, H.S., Ting, J., Okino, K.H., Morris, C.F., McNiece, I.K., Jacobsen, F.W., Mendiaz, E.A., and et al. (1990). Primary structure and functional expression of rat and human stem cell factor DNAs. Cell *63*, 203-211. 10.1016/0092-8674(90)90301-t.

29. Huang, E.J., Nocka, K.H., Buck, J., and Besmer, P. (1992). Differential expression and processing of two cell associated forms of the kit-ligand: KL-1 and KL-2. Mol Biol Cell *3*, 349-362. 10.1091/mbc.3.3.349.

30. Flanagan, J.G., Chan, D.C., and Leder, P. (1991). Transmembrane form of the kit ligand growth factor is determined by alternative splicing and is missing in the Sld mutant. Cell *64*, 1025-1035. 10.1016/0092-8674(91)90326-t.

31. Langley, K.E., Mendiaz, E.A., Liu, N., Narhi, L.O., Zeni, L., Parseghian, C.M., Clogston, C.L., Leslie, I., Pope, J.A., Lu, H.S., and et al. (1994). Properties of variant forms of human stem cell factor recombinantly expressed in Escherichia coli. Arch Biochem Biophys *311*, 55-61. 10.1006/abbi.1994.1208.

32. Nitta, K., Matsuzaki, Y., Konno, A., and Hirai, H. (2017). Minimal Purkinje Cell-Specific PCP2/L7 Promoter Virally Available for Rodents and Non-human Primates. Mol Ther Methods Clin Dev *6*, 159-170. 10.1016/j.omtm.2017.07.006.

33. Zaman, T., Lee, K., Park, C., Paydar, A., Choi, J.H., Cheong, E., Lee, C.J., and Shin, H.S. (2011). Cav2.3 channels are critical for oscillatory burst discharges in the reticular thalamus and absence epilepsy. Neuron *70*, 95-108. 10.1016/j.neuron.2011.02.042.

34. Maricich, S.M., and Herrup, K. (1999). Pax-2 expression defines a subset of GABAergic interneurons and their precursors in the developing murine cerebellum. J Neurobiol *41*, 281-294. 10.1002/(sici)1097-4695(19991105)41:2<281::aid-neu10>3.0.co;2-5.

35. Blake, J.A., and Ziman, M.R. (2014). Pax genes: regulators of lineage specification and progenitor cell maintenance. Development *141*, 737-751. 10.1242/dev.091785.

36. Pfeffer, P.L., Payer, B., Reim, G., di Magliano, M.P., and Busslinger, M. (2002). The activation and maintenance of Pax2 expression at the mid-hindbrain boundary is controlled by separate enhancers. Development *129*, 307-318. 10.1242/dev.129.2.307.

37. Lee, S.B., Doberstein, K., Baumgarten, P., Wieland, A., Ungerer, C., Burger, C., Hardt, K., Boehncke, W.H., Pfeilschifter, J., Mihic-Probst, D., et al. (2011). PAX2 regulates ADAM10 expression and mediates anchorage-independent cell growth of melanoma cells. PLoS One *6*, e22312. 10.1371/journal.pone.0022312.

38. Wehrle-Haller, B. (2003). The role of Kit-ligand in melanocyte development and epidermal homeostasis. Pigment Cell Res *16*, 287-296. 10.1034/j.1600-0749.2003.00055.x.

39. Besmer, P., Manova, K., Duttlinger, R., Huang, E.J., Packer, A., Gyssler, C., and Bachvarova, R.F. (1993). The kit-ligand (steel factor) and its receptor c-kit/W: pleiotropic roles in gametogenesis and melanogenesis. Dev Suppl, 125-137.

40. Zhou, J., Brown, A.M., Lackey, E.P., Arancillo, M., Lin, T., and Sillitoe, R.V. (2020). Purkinje cell neurotransmission patterns cerebellar basket cells into zonal modules defined by distinct pinceau sizes. Elife *9*. 10.7554/eLife.55569.

41. Zhang, B., Chen, L.Y., Liu, X., Maxeiner, S., Lee, S.J., Gokce, O., and Sudhof, T.C. (2015). Neuroligins Sculpt Cerebellar Purkinje-Cell Circuits by Differential Control of Distinct Classes of Synapses. Neuron *87*, 781-796. 10.1016/j.neuron.2015.07.020.

42. Liu, Z., Jiang, M., Liakath-Ali, K., Sclip, A., Ko, J., Zhang, R.S., and Sudhof, T.C. (2022). Deletion of Calsyntenin-3, an atypical cadherin, suppresses inhibitory synapses but increases excitatory parallel-fiber synapses in cerebellum. Elife *11*. 10.7554/eLife.70664.

43. Chan-Palay, V. (1971). The recurrent collaterals of Purkinje cell axons: a correlated study of the rat's cerebellar cortex with electron microscopy and the Golgi method. Z Anat Entwicklungsgesch *134*, 200-234. 10.1007/BF00519300.

44. Larramendi, L.M., and Lemkey-Johnston, N. (1970). The distribution of recurrent Purkinje collateral synapses in the mouse cerebellar cortex: an electron microscopic study. J Comp Neurol *138*, 451-459. 10.1002/cne.901380405.

45. Orduz, D., and Llano, I. (2007). Recurrent axon collaterals underlie facilitating synapses between cerebellar Purkinje cells. Proc Natl Acad Sci U S A *104*, 17831-17836. 10.1073/pnas.0707489104.

46. Witter, L., Rudolph, S., Pressler, R.T., Lahlaf, S.I., and Regehr, W.G. (2016). Purkinje Cell Collaterals Enable Output Signals from the Cerebellar Cortex to Feed Back to Purkinje Cells and Interneurons. Neuron *91*, 312-319. 10.1016/j.neuron.2016.05.037.

47. Kreitzer, A.C., Carter, A.G., and Regehr, W.G. (2002). Inhibition of interneuron firing extends the spread of endocannabinoid signaling in the cerebellum. Neuron *34*, 787-796. 10.1016/s0896-6273(02)00695-5.

48. Kreitzer, A.C., and Regehr, W.G. (2001). Cerebellar depolarization-induced suppression of inhibition is mediated by endogenous cannabinoids. J Neurosci *21*, RC174. 10.1523/JNEUROSCI.21-20-j0005.2001.

49. Safo, P.K., Cravatt, B.F., and Regehr, W.G. (2006). Retrograde endocannabinoid signaling in the cerebellar cortex. Cerebellum *5*, 134-145. 10.1080/14734220600791477.

50. Williams, M.R., Fuchs, J.R., Green, J.T., and Morielli, A.D. (2012). Cellular mechanisms and behavioral consequences of Kv1.2 regulation in the rat cerebellum. J Neurosci *32*, 9228-9237. 10.1523/JNEUROSCI.6504-11.2012.

51. Fuchs, J.R., Robinson, G.M., Dean, A.M., Schoenberg, H.E., Williams, M.R., Morielli, A.D., and Green, J.T. (2014). Cerebellar secretin modulates eyeblink classical conditioning. Learn Mem *21*, 668-675. 10.1101/lm.035766.114.

52. Wu, W.Y., Liu, Y., Wu, M.C., Wang, H.W., Chu, C.P., Jin, H., Li, Y.Z., and Qiu, D.L. (2020). Corticotrophin-Releasing Factor Modulates the Facial Stimulation-Evoked Molecular Layer Interneuron-Purkinje Cell Synaptic Transmission in vivo in Mice. Front Cell Neurosci *14*, 563428. 10.3389/fncel.2020.563428.

53. Zhou, H., Lin, Z., Voges, K., Ju, C., Gao, Z., Bosman, L.W., Ruigrok, T.J., Hoebeek, F.E., De Zeeuw, C.I., and Schonewille, M. (2014). Cerebellar modules operate at different frequencies. Elife *3*, e02536. 10.7554/eLife.02536.

54. Brochu, G., Maler, L., and Hawkes, R. (1990). Zebrin II: a polypeptide antigen expressed selectively by Purkinje cells reveals compartments in rat and fish cerebellum. J Comp Neurol *291*, 538-552. 10.1002/cne.902910405.

55. Leclerc, N., Dore, L., Parent, A., and Hawkes, R. (1990). The compartmentalization of the monkey and rat cerebellar cortex: zebrin I and cytochrome oxidase. Brain Res *506*, 70-78. 10.1016/0006-8993(90)91200-z.

56. Sarna, J.R., Marzban, H., Watanabe, M., and Hawkes, R. (2006). Complementary stripes of phospholipase Cbeta3 and Cbeta4 expression by Purkinje cell subsets in the mouse cerebellum. J Comp Neurol *496*, 303-313. 10.1002/cne.20912.

57. Marzban, H., Chung, S., Watanabe, M., and Hawkes, R. (2007). Phospholipase Cbeta4 expression reveals the continuity of cerebellar topography through development. J Comp Neurol *502*, 857-871. 10.1002/cne.21352.

58. Adachi, S., Ebi, Y., Nishikawa, S., Hayashi, S., Yamazaki, M., Kasugai, T., Yamamura, T., Nomura, S., and Kitamura, Y. (1992). Necessity of extracellular domain of W (c-kit) receptors for attachment of murine cultured mast cells to fibroblasts. Blood *79*, 650-656.

59. Tabone-Eglinger, S., Calderin-Sollet, Z., Pinon, P., Aebischer, N., Wehrle-Haller, M., Jacquier, M.C., Boettiger, D., and Wehrle-Haller, B. (2014). Niche anchorage and signaling through membrane-bound Kit-ligand/c-kit receptor are kinase independent and imatinib insensitive. FASEB J *28*, 4441-4456. 10.1096/fj.14-249425.

60. Ango, F., di Cristo, G., Higashiyama, H., Bennett, V., Wu, P., and Huang, Z.J. (2004). Ankyrin-based subcellular gradient of neurofascin, an immunoglobulin family protein, directs GABAergic innervation at purkinje axon initial segment. Cell *119*, 257-272. 10.1016/j.cell.2004.10.004.

61. Buttermore, E.D., Piochon, C., Wallace, M.L., Philpot, B.D., Hansel, C., and Bhat, M.A. (2012). Pinceau organization in the cerebellum requires distinct functions of neurofascin in Purkinje and basket neurons during postnatal development. J Neurosci *32*, 4724-4742. 10.1523/JNEUROSCI.5602-11.2012.

62. Telley, L., Cadilhac, C., Cioni, J.M., Saywell, V., Jahannault-Talignani, C., Huettl, R.E., Sarrailh-Faivre, C., Dayer, A., Huber, A.B., and Ango, F. (2016). Dual Function of NRP1 in Axon Guidance and Subcellular Target Recognition in Cerebellum. Neuron *91*, 1276-1291. 10.1016/j.neuron.2016.08.015.

63. Cioni, J.M., Telley, L., Saywell, V., Cadilhac, C., Jourdan, C., Huber, A.B., Huang, J.Z., Jahannault-Talignani, C., and Ango, F. (2013). SEMA3A signaling controls layer-specific interneuron branching in the cerebellum. Curr Biol *23*, 850-861. 10.1016/j.cub.2013.04.007.

64. Wu, W.C., Bradley, S.P., Christie, J.M., and Pugh, J.R. (2022). Mechanisms and Consequences of Cerebellar Purkinje Cell Disinhibition in a Mouse Model of Duchenne Muscular Dystrophy. J Neurosci *42*, 2103-2115. 10.1523/JNEUROSCI.1256-21.2022.

65. Wisden, W., Murray, A.J., McClure, C., and Wulff, P. (2009). Studying Cerebellar Circuits by Remote Control of Selected Neuronal Types with GABA(A) Receptors. Front Mol Neurosci *2*, 29. 10.3389/neuro.02.029.2009.

66. Bonnan, A., Zhang, K., Gaffield, M.A., and Christie, J.M. (2023). Expression of a Form of Cerebellar Motor Memory Requires Learned Alterations to the Activity of Inhibitory Molecular Layer Interneurons. J Neurosci *43*, 601-612. 10.1523/JNEUROSCI.0731-22.2022.

67. Gaffield, M.A., Rowan, M.J.M., Amat, S.B., Hirai, H., and Christie, J.M. (2018). Inhibition gates supralinear Ca(2+) signaling in Purkinje cell dendrites during practiced movements. Elife *7*. 10.7554/eLife.36246.

68. Motro, B., Wojtowicz, J.M., Bernstein, A., and van der Kooy, D. (1996). Steel mutant mice are deficient in hippocampal learning but not long-term potentiation. Proc Natl Acad Sci U S A *93*, 1808-1813. 10.1073/pnas.93.5.1808.

69. Katafuchi, T., Li, A.J., Hirota, S., Kitamura, Y., and Hori, T. (2000). Impairment of spatial learning and hippocampal synaptic potentiation in c-kit mutant rats. Learn Mem *7*, 383-392. 10.1101/lm.33900.

70. Kondo, T., Katafuchi, T., and Hori, T. (2002). Stem cell factor modulates paired-pulse facilitation and long-term potentiation in the hippocampal mossy fiber-CA3 pathway in mice. Brain Res *946*, 179-190. 10.1016/s0006-8993(02)02879-2.